6 Heterojunction and Devices

6.1 Heterojunction

PN junction made of the same type of semiconductor as described in section 3.1 is called a homojunction. On the other hand, a junction made of different types of semiconductors is called a heterojunction. Since a heterojunction is a junction between semiconductors with different bandgap energies E_G and electron affinities χ, the appearance of the energy band structure is different from that of a homojunction, and the electrical properties are also different.

To make heterojunctions, not just any material can be used, but they must have a similar crystal structure and lattice constants to avoid crystal defects. Figure 6.1 shows the bandgap energy E_G and lattice constant of $GaAs$- and InP-based semiconductors (sphalerite crystals). The Figure also shows for Si and Ge semiconductors for reference. In addition, Figure 6.2 shows the E_G and lattice constant of GaN-based semiconductors (wurtzite-type crystals). The Figure also shows for a $4HSiC$ semiconductor for reference.

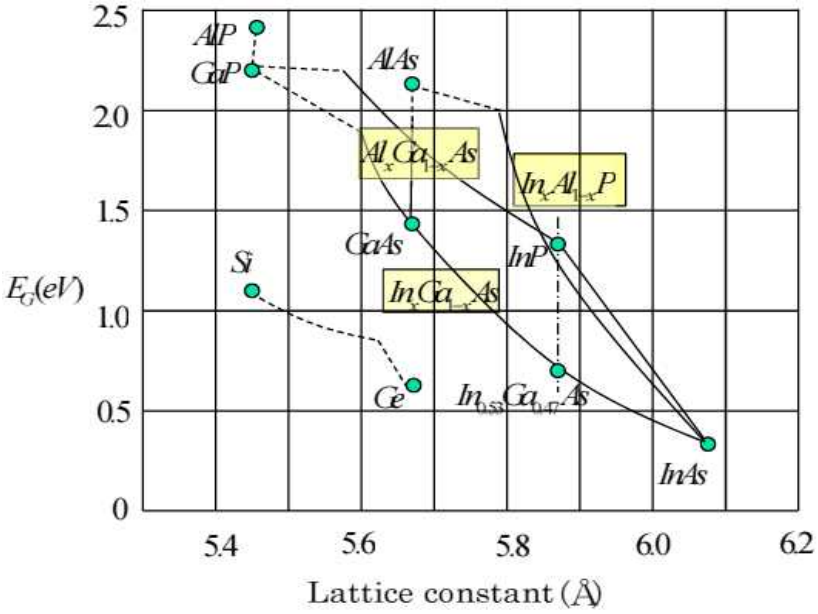

Figure 6.1 E_G and lattice constant of $GaAs$- and InP-based semiconductors (Data from Ref. [9], p. 44)

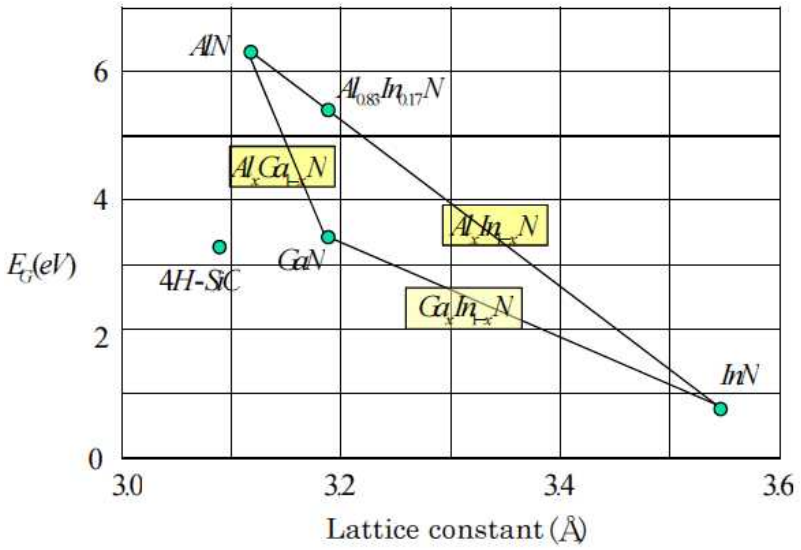

Figure 6.2 E_G and lattice constant of GaN-based semiconductors
(Data from Ref. [14], p. 5)

Figure 6.3 shows the band gap energy E_G and electron affinity χ for these semiconductor materials.

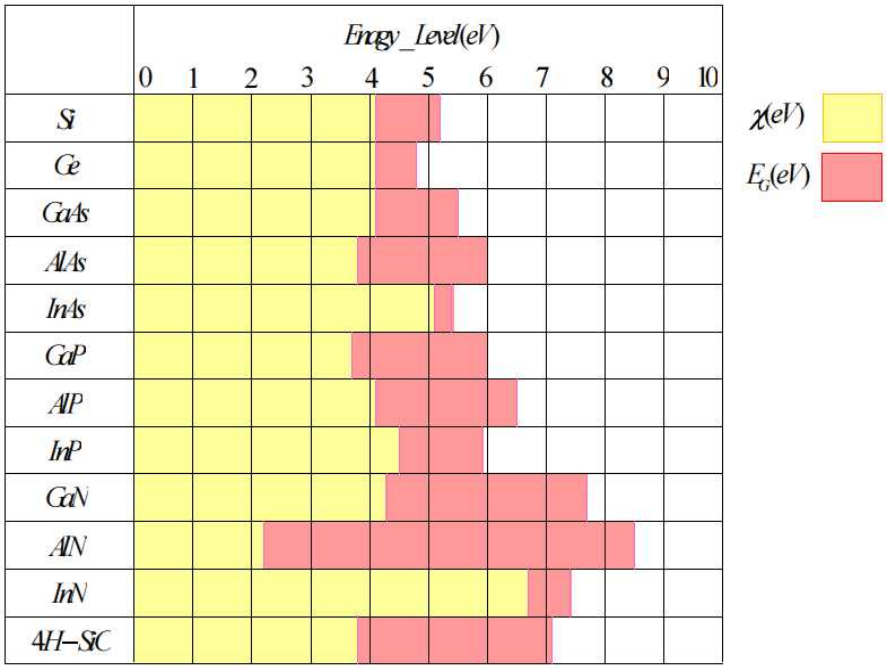

Figure 6.3 E_G and χ for semiconductor materials
(χ data from Ref. [12], p. 1079)

Figures 6.4(a) and (b) show the appearance of the energy band structure of a $Al_{0.3}Ga_{0.7}As/GaAs$ heterojunction as an example of a heterojunction. From Figure 6.1, the lattice constants of $Al_{0.3}Ga_{0.7}As$ and $GaAs$ are almost identical and the junction can be formed without crystal defects. Figure 6.4(a) shows the case where $Al_{0.3}Ga_{0.7}As$ is an N-type ($nAl_{0.3}Ga_{0.7}As$) and $GaAs$ is a P-type ($pGaAs$). The figure also shows the homojunction assumption as a two-dotted line for reference. On the other hand, Figure 6.4(b) shows the case where $Al_{0.3}Ga_{0.7}As$ is a high concentration N-type ($n^+Al_{0.3}Ga_{0.7}As$) and $GaAs$ is non-doped ($iGaAs$). In this case, the Fermi energy level crosses the triangular potential well at the discontinuity of the heterojunction, where a high density of conduction electrons is generated. As a result, a channel is formed in which the conduction electrons are carriers. As the channel is extremely thin ($5\sim9nm$), the electrons in the channel are called 2-Dimensional Electron Gas ($2DEG$).

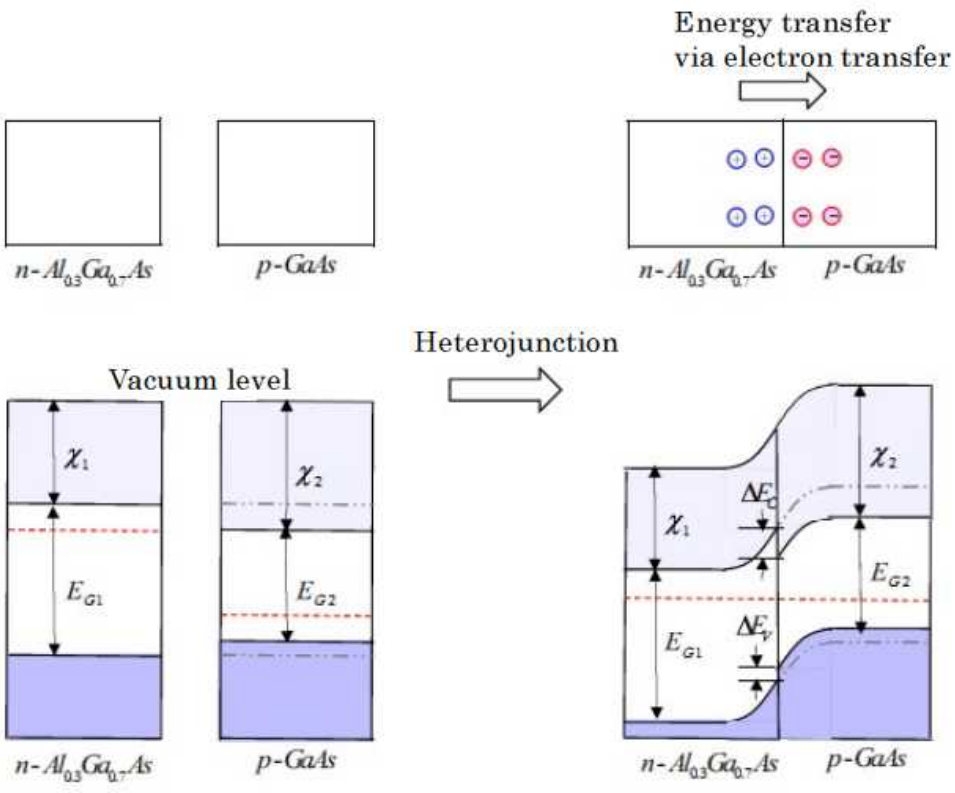

Figure 6.4(a) Energy band structure of $Al_{0.3}Ga_{0.7}As/GaAs$ heterojunction (for $nAl_{0.3}Ga_{0.7}As/pGaAs$ heterojunction)

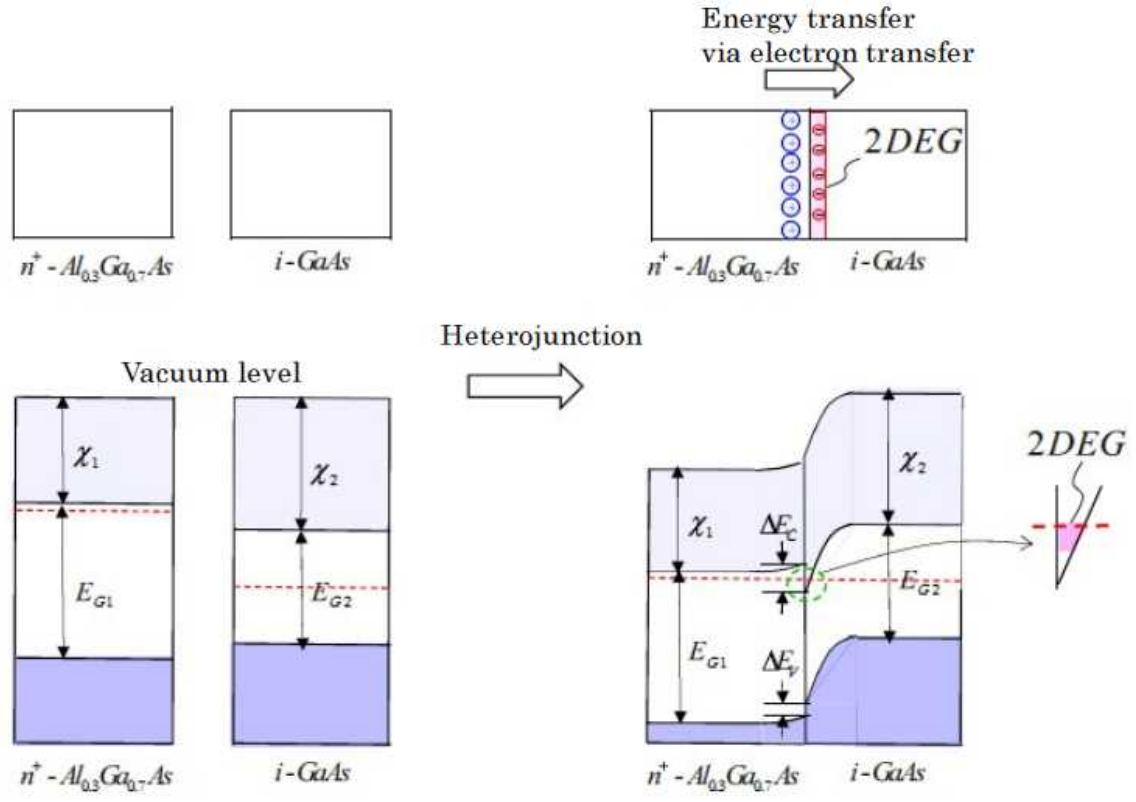

Figure 6.4(b) Energy band structure of $Al_{0.3}Ga_{0.7}As/GaAs$ heterojunction (for $n^+Al_{0.3}Ga_{0.7}As/iGaAs$ heterojunction)

Next, consider a junction consisting of a Schottky-bonded metal ($Metal$), a highly concentrated N- type $Al_{0.3}Ga_{0.7}As$ ($n^+Al_{0.3}Ga_{0.7}As$) and a non-doped $GaAs$ ($iGaAs$). Here, the $n^+Al_{0.3}Ga_{0.7}As$ part is called the barrier layer and the $iGaAs$ part is called the channel layer. When studying this junction, it is considered as follows. Namely, the Schottky junction of the metal ($Metal$) and the barrier layer (in this case $n^+Al_{0.3}Ga_{0.7}As$) is considered as device-1, the channel layer (in this case $iGaAs$) as device-2, and consider that devices-1 and -2 make a heterojunction. Here, the $n^+Al_{0.3}Ga_{0.7}As$ part of device-1 has been partially depleted by ionised donors (positive charge). The original Fermi energy level E_{f1} of device-1 is higher than the original Fermi energy level E_{f2} of device-2 by $\Delta E^0(=E_{f1}-E_{f2})$. Therefore, electrons are transferred from the device-1 side to the device-2 side during junction, which causes the Fermi energy levels of both devices to change so that they are equal, resulting in a thermal equilibrium state. The energy band structure will change (curve) in response to changes in Fermi energy levels. Figure 6.5

shows the energy band structure of a $Metal/n^{+}Al_{0.3}Ga_{0.7}As/iGaAs$ junction consisting of a junction of devices-1 and -2. The $Metal/n^{+}Al_{0.3}Ga_{0.7}As$ junction is a Schottky junction and the $n^{+}Al_{0.3}Ga_{0.7}As/iGaAs$ junction is a heterojunction.

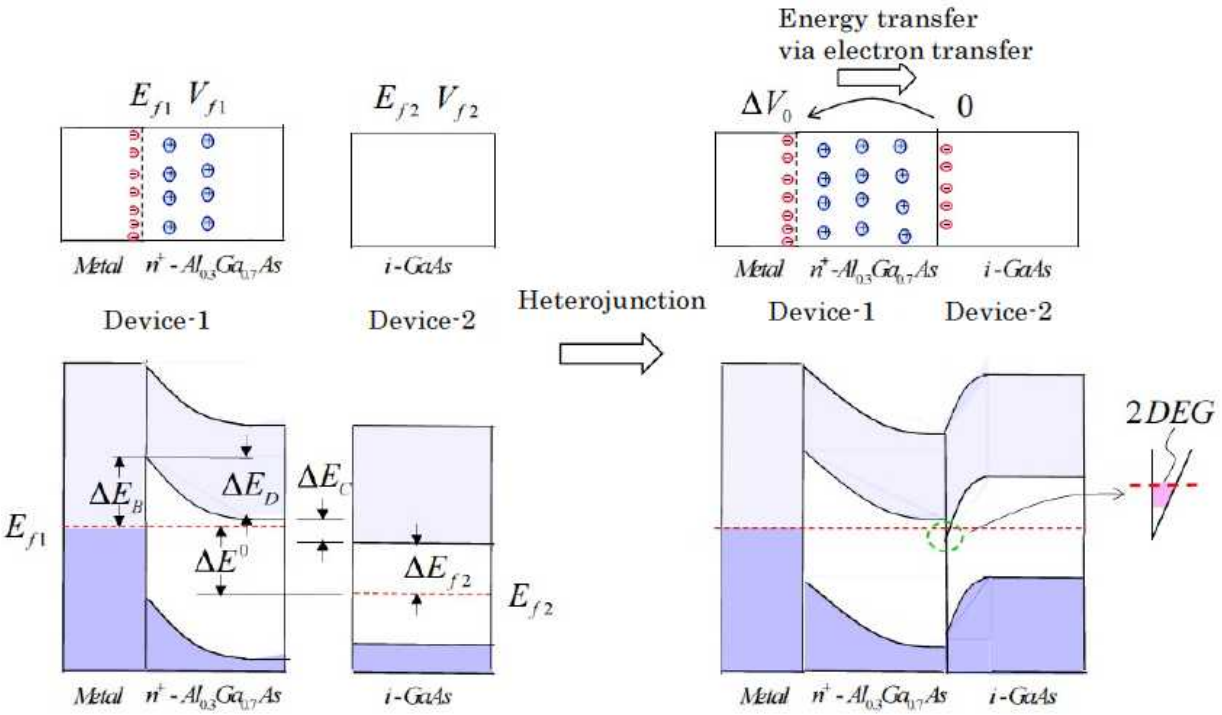

Figure 6.5 Energy band structure of a $Metal/n^{+}Al_{0.3}Ga_{0.7}As/iGaAs$ junction consisting of a junction of devices-1 and -2.

The energy difference ΔE^0 originally possessed between devices-1 and -2 can be related to the potential difference ΔV^0 as follows.

$$\Delta E^0 = E_{f1} - E_{f2} = -eV_{f1} + eV_{f2} = -e\Delta V^0 \qquad (6.1)$$

where $\Delta V^0 = V_{f1} - V_{f2}$

The junction causes the transfer of electrons from device-1 to device-2, creating a potential difference ΔV_0 at the junction, and the originally existing potential difference ΔV^0 is cancelled out by ΔV_0, resulting in a potential difference of zero and, consequently, a thermal equilibrium state

with an energy difference of zero. The equation is expressed as follows.

$$\delta V = \Delta V^0 + \Delta V_0 = 0 \longrightarrow \Delta V_0 = -\Delta V^0 \tag{6.2}$$

$$\delta E = \Delta E^0 + \Delta E_0 = -e(\Delta V^0 + \Delta V_0) = 0 \longrightarrow \Delta E_0 = -\Delta E^0 \tag{6.3}$$

note that $\Delta E^0 = -e\Delta V^0 \geq 0$ and $\Delta E_0 = -e\Delta V_0 \leq 0$

Here, ΔE^0 can be expressed using the energy variables in Figure 6.5 as follows.

$$\Delta E^0 = -e\Delta V^0 = -\Delta E_B + \Delta E_D + \Delta E_C + \Delta E_{f2} \tag{6.4}$$

From this we obtain the following equation for the potential difference.

$$\begin{aligned} \Delta V_0 = -\Delta V^0 &= \frac{1}{e}(-\Delta E_B + \Delta E_D + \Delta E_C + \Delta E_{f2}) \\ &= -\frac{\Delta E_B}{e} + \frac{eN_D}{2\varepsilon_1} d^2 + \frac{\Delta E_C}{e} + \frac{\Delta E_{f2}}{e} \end{aligned} \tag{6.5}$$

Where d is the thickness of the barrier layer, ε_1 is the dielectric constant and N_D is the donor density. Other energy variables $\Delta E_B, \Delta E_C, \Delta E_{f2}$ are determined from the Fermi energy levels and electron affinities of the metal and semiconductors. The relation $\frac{\Delta E_D}{e} = \frac{eN_D}{2\varepsilon_1} d^2$ in the second term of the right-hand side of the above equation is derived by assuming that the entire barrier layer ($n^+Al_{0.3}Ga_{0.7}As$) is depletion-layered and using chapter 4 on Schottky junctions, equation (4.6).

Next, consider applying a bias voltage V_G to the device-1 side (device-2 side is grounded). Figure 6.6 shows how the energy band structure changes when a bias voltage V_G is applied to the $Metal/n^+Al_{0.3}Ga_{0.7}As/iGaAs$ heterojunction and the Fermi energy level is changed ($\Delta E_V = -eV_G$).

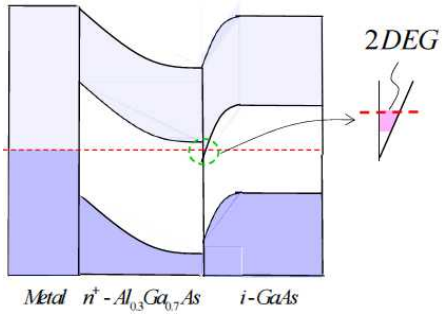

(a) $V_G = 0$ (thermal equilibrium)

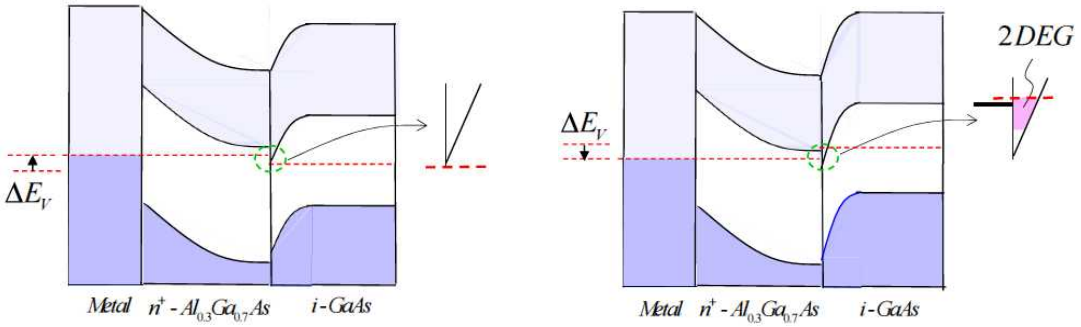

(b) $V_G < 0$ (c) $V_G > 0$

Figure 6.6 Energy band structure of a heterojunction when bias voltage V_G is applied.

In this case, the potential difference at the junction between devices-1 and -2 is $\Delta V_0 (= -\Delta V^0) \rightarrow V_G + \Delta V_0 (= V_G - \Delta V^0)$, and the following equation is obtained from equation (6.5).

$$V_G + \Delta V_0 = V_G - \Delta V^0 = V_G + (-\frac{\Delta E_B}{e} + \frac{eN_D}{2\varepsilon_1} d^2 + \frac{\Delta E_C}{e} + \frac{\Delta E_{f2}}{e}) \qquad (6.6)$$

In Figures 6.5 and 6.6, what happens to the amount of charge (per unit area) Q_I of $2DEG$ present at the junction of $iGaAs$? Assuming that all the donors in $n^+ Al_{0.3}Ga_{0.7}As$ are ionised and all depleted, this part behaves as a parallel plate capacitor with thickness d and its (per unit area) capacitance is given by $C_{ox} = \frac{\varepsilon_1}{d}$. Figure 6.7 shows the junction configuration and capacitance model.

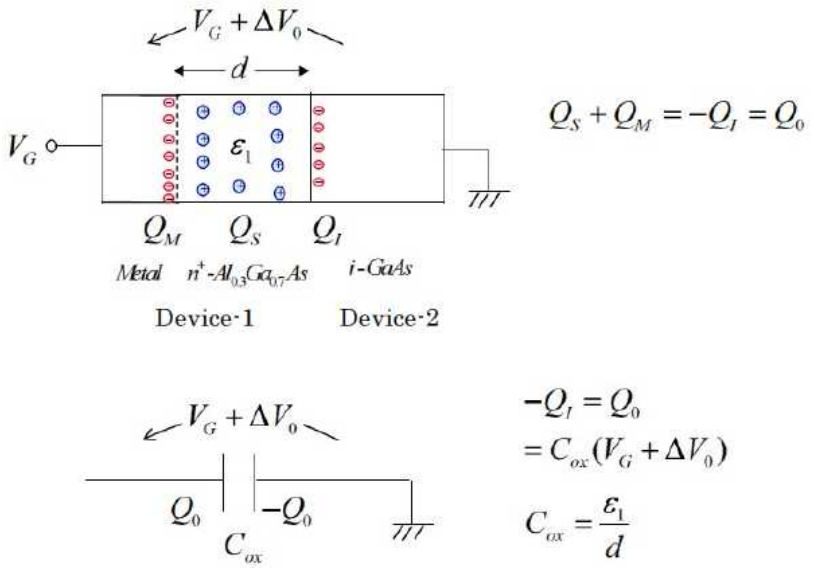

Figure 6.7 Junction configuration and capacitance model

The following relationship exists between the surface charge Q_M of the metal, the depletion layer charge Q_S of the $n^+ Al_{0.3}Ga_{0.7}As$ semiconductor and the charge Q_I due to the $2DEG$ of the $iGaAs$ semiconductor.

$$Q_S + Q_M = -Q_I = Q_0 \tag{6.7}$$

From this, when given the voltage $V_G + \Delta V_0 (= V_G - \Delta V^{\oplus})$ across the capacitor, Q_I can be obtained from the following equation.

$$\begin{aligned} -Q_I &= Q_0 = C_{ox}(V_G + \Delta V_0) \\ &= \frac{\varepsilon_1}{d}\left(V_G + (-\frac{\Delta E_B}{e} + \frac{eN_D}{2\varepsilon_1} d^2 + \frac{\Delta E_C}{e} + \frac{\Delta E_{f2}}{e}) \right) \end{aligned} \tag{6.8}$$

In equation (6.8), since $\Delta V_0 \geq 0$, (a) Q_I has a finite value even when no bias is applied ($V_G = 0$), as a result, a $2DEG$ channel is present (normally on). (b) When a negative bias voltage $V_G (< 0)$ is applied, $Q_0 = -Q_I$ decreases and eventually reaches 0. At this time, the channel by$2DEG$ is lost and pinch-off (depletion mode operation). (c) On the other hand, $Q_0 = -Q_I$ increases for a while when $V_G (> 0)$ is applied, but there is a limit. This is because as V_G is

increased, the Fermi energy level of $iGaAs$ becomes higher than the bottom of the conduction band of $n^{+}Al_{0.3}Ga_{0.7}As$, causing charge to flow out from the device-2 side to the device-1 side.

6.2 Heterojunction FET (HFET)

6.2.1 HEMT

HEMT (High Electron Mobility Transistor) [16] can be considered a FET with a heterojunction at the junction. Figure 6.8 shows a structure model of a HEMT with an $Al_{0.3}Ga_{0.7}As/GaAs$ heterojunction. Note that the energy band structure of the junction is as shown in Figure 6.5.

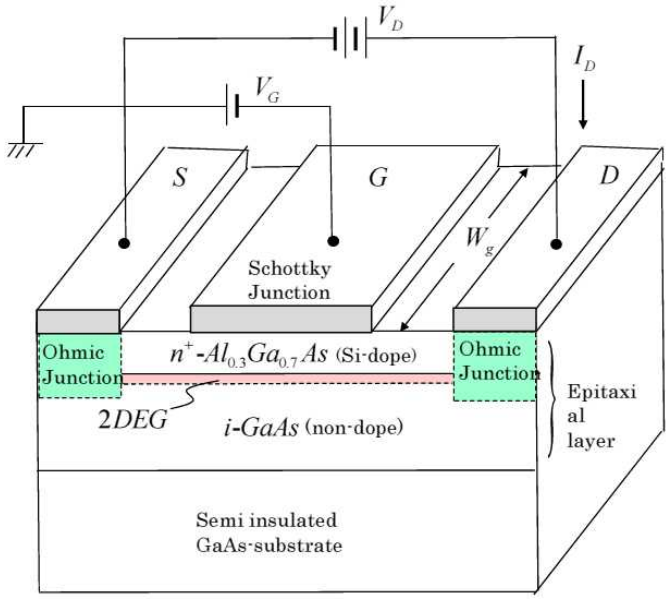

Figure 6.8 $Al_{0.3}Ga_{0.7}As/GaAs$ HEMT structure model.

HEMT consists of an epitaxial layer of $n^{+}Al_{0.3}Ga_{0.7}As/iGaAs$ hetero- junction formed on a semi-insulating GaAs substrate with source (S), drain (D) and gate (G) terminals. The S and D terminals are connected to the i-$GaAs$ by an ohmic junction and the gate section consists of a Schottky junction + heterojunction made up of $Metal/n^{+}Al_{0.3}Ga_{0.7}As/iGaAs$ shown in Fig. 6.5. A channel is formed by $2DEG$ in the $iGaAs$ junction and a drain current I_D flows between S and D. The amount of $2DEG$ changes according to the

voltage V_G applied between G and S, and I_D is controlled.

A quantitative analysis of the operation is presented below. Let the y-axis be the channel direction of the semiconductor, with the right end on the S side as the origin ($y = 0$) and the left end on the D side as $y = L_g$. The potential at $y = 0$ is $V(0) = 0$ and $V(L_g) = V_D$ at $y = L_g$. The gate width is W_g. Consider applying a gate voltage V_G ($0 \geq V_G \geq -\Delta V_0$) as well as a small (linear region) drain voltage V_D and letting a drain current I_D flow. The potential $V(y)$ in the channel is given as a function of position y, from which the amount of charge per unit area $Q_I(y)$ at y is given by

$$Q_I(y) = -C_{ox}(V_G + \Delta V_0 - V(y)) \tag{6.9}$$

The drain current I_D (positive in the direction of flow from drain to source) can be regarded as a drift current due to carriers (conduction electrons) in the channel and is given by

$$I_D = -W_g \mu_e Q_I(y) \frac{dV}{dy} \tag{6.10}$$

From the above equation,

$$I_D dy = W_g \mu_e C_{ox}(V_G + \Delta V_0 - V(y))dV \tag{6.11}$$

Integrating the left-hand side with $y = 0 \rightarrow L_g$ and the right-hand side with $V = 0 \rightarrow V_D$ ($V(0) \rightarrow V(L_g)$) yields the following equation.

$$I_D = \frac{W_g \mu_e C_{ox}}{L_g}\left((V_G + \Delta V_0)V_D - \frac{1}{2}V_D^2\right)$$
$$= -\frac{1}{2}\frac{W_g \mu_e C_{ox}}{L_g}\left[\left(V_D - (V_G + \Delta V_0)\right)^2 - (V_G + \Delta V_0)^2\right] \quad (6.12)$$

The left-hand side integral uses the fact that I_D is constant regardless of location due to the continuity of the current. Equation (6.12) is valid for $0 \leq V_D \leq V_P = V_G + \Delta V_0$ (V_P is the pinch-off voltage). As V_D is increased and $V_D = V_P = V_G + \Delta V_0$, the charge becomes $Q_i = 0$ at $y = L_g$ from equation (6.9) (it pinches off). When $V_D \geq V_P$, the excess voltage is used in the high resistance part due to channel disappearance and, as an approximation, the configuration of the channel under the gate remains unchanged. From this, it follows that I_D is constant for $V_D \geq V_P$. Figure 6.9 shows the $I_D - V_D$ characteristics of the HEMT.

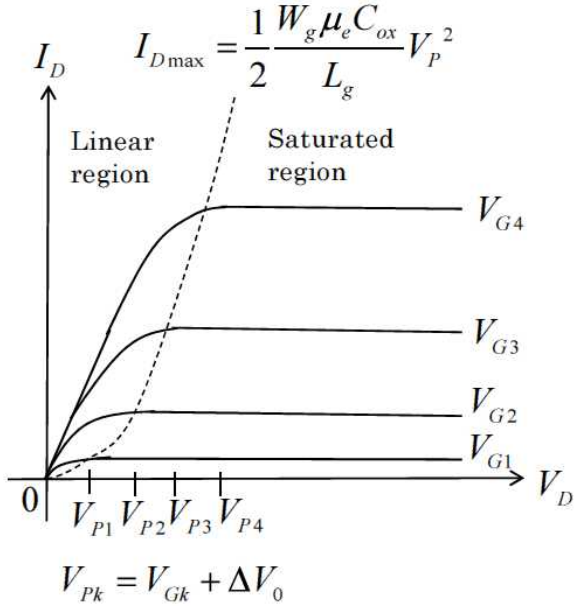

Figure 6.9 I-V characteristics of HEMT.

The maximum current I_{Dmax} when V_G is applied is obtained when $V_D = V_P = V_G + \Delta V_0$ and is given by the following equation, where the characteristic of I_{Dmax} gives the pinch-off curve.

$$I_{D\max} = \frac{1}{2}\frac{W_g \mu_e C_{ox}}{L_g}(V_G + \Delta V_0)^2 = \frac{1}{2}\frac{W_g \mu_e C_{ox}}{L_g} V_P^{\,2} \tag{6.13}$$

The mutual conductance g_m in the saturation region ($V_D \geq V_P$) is given by

$$g_m = \frac{\partial I_{D\max}}{\partial V_G} = \frac{W_g \mu_e C_{ox}}{L_g}(V_G + \Delta V_0) \tag{6.14}$$

If the capacitance C_{ox} in the $n^+ Al_{0.3}Ga_{0.7}As$ part contributes all to the gate-source capacitance C_{gs}, then C_{gs} is given by

$$C_{gs} = L_g W_g C_{ox} = \frac{\varepsilon_1 L_g W_g}{d} \tag{6.15}$$

Using g_m and C_{gs} (ignoring all other parasitic elements), the small- signal RF equivalent circuit of the HEMT can be represented as in Figure 6.10.

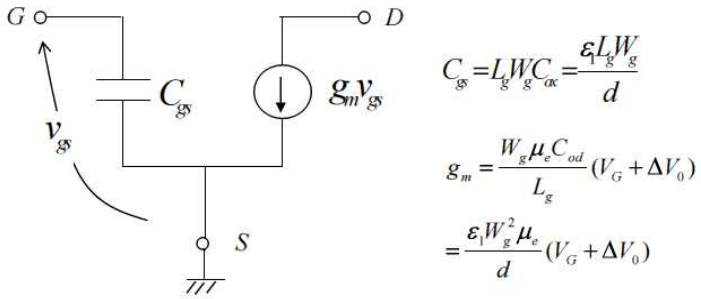

Figure 6.10 Small-signal RF equivalent circuit of HEMT
(not including parasitic elements)

From the equivalent circuit, the source ground (common source) current gain β and cut-off frequency f_T are given by

$$\beta = \frac{g_m}{j\omega C_{gs}} = \frac{\mu_e}{j\omega L_g^2}(V_G + \Delta V_0) \tag{6.16}$$

$$f_T = \frac{\mu_e}{2\pi L_g^2}(V_G + \Delta V_0) \tag{6.17}$$

To increase β, f_T, it is necessary to shorten the gate length L_g and increase the electron mobility μ_e. In HEMTs, the channel layer is made of high-purity $GaAs$ ($iGaAs$), which can increase the μ_e compared to MESFETs that use $nGaAs$ with impurities in the channel part. Structures that can further increase μ_e include pHEMTs and InP HEMTs, which are discussed below. According to equations (6.16) and (6.17), the contribution of the barrier layer thickness d is not apparent in terms of higher gain and higher frequency, but according to equation (6.13), an increase in $C_{ox}(=\frac{\varepsilon_1}{d})$ is necessary to increase the current density for higher output power, which in turn requires a reduction in d.

6.2.2 pseudomorphic-HEMT (pHEMT)

pHEMT (pseudo morphic HEMT) is an improved version of the HEMT for higher performance. Figure 6.11 shows the structure model of a pHEMT with $n^+Al_{0.3}Ga_{0.7}As/iIn_{0.2}Ga_{0.8}As/iGaAs$ heterojunction and Figure 6.12 shows its energy band structure. pHEMT has a structure with a $iIn_{0.2}Ga_{0.8}As$ layer between the $n^+Al_{0.3}Ga_{0.7}As$ and $iGaAs$ of a conventional HEMT. This allows the triangular potential wells formed at the heterojunction to be deeper, resulting in a higher electron density of the $2DEG$. In addition, since the electron mobility μ_e of $iIn_{0.2}Ga_{0.8}As$, where the channel is formed, is larger than that of $iGaAs$, higher speed and gain can be achieved. From a manufacturing standpoint, the advantage is that pHEMT can be fabricated simply by adding an $iIn_{0.2}Ga_{0.8}As$ layer process to the conventional HEMT manufacturing process. In general, μ_e increases as the composition of In (the value of x) in $In_xGa_{1-x}As$ mixed semiconductor increases. However, as the value of x increases, the difference in lattice constants between

$In_xGa_{1-x}As$ and $GaAs$ (and $Al_{0.3}Ga_{0.7}As$) increases (see Figure 6.1), and lattice defects due to distortion tend to occur in the crystal. Therefore, it is necessary to choose a value of x in a range which can absorb the distortion problem, and a value of around $x \approx 0.2$ is adopted. In this structure, there is distortion at the junction, so it is called pseudo morphic HEMT (pHEMT).

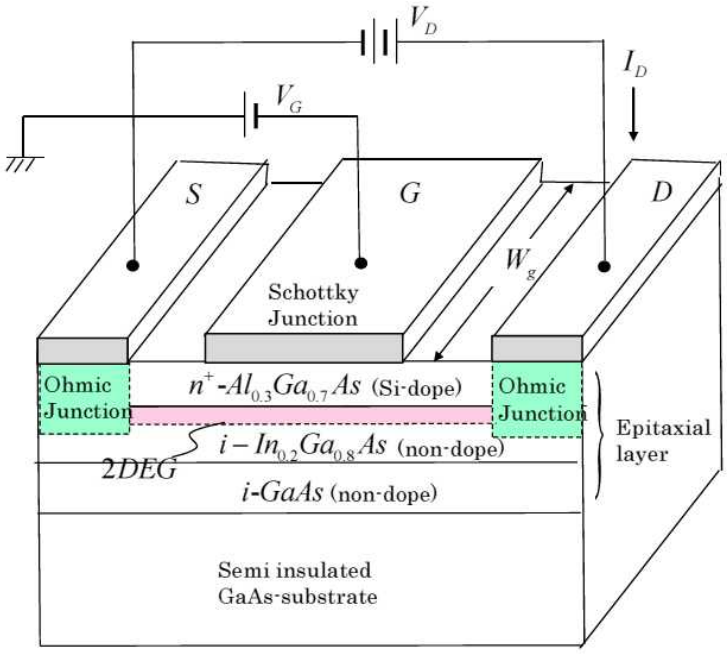

Figure 6.11 Structure model of $Al_{0.3}Ga_{0.7}As/In_{0.2}Ga_{0.8}As/GaAs$ pHEMT

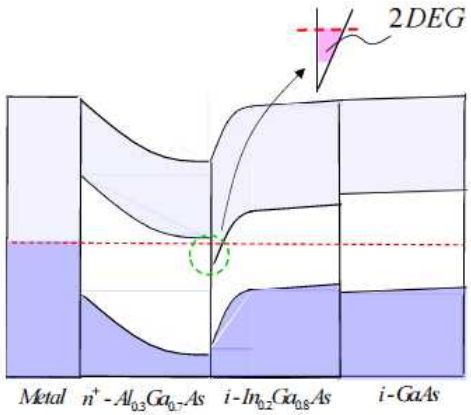

Figure 6.12 Energy band structure of $Al_{0.3}Ga_{0.7}As/In_{0.2}Ga_{0.8}As/GaAs$ pHEMT

6.2.3 InP HEMT

By using $In_xGa_{1-x}As$ with larger In composition (value of x), larger electron mobility μ_e can be obtained, enabling higher speed and gain. As a device that can use $In_xGa_{1-x}As$ with a large In composition in the channel layer, InPHEMT is available. Figure 6.13 shows the structure model of the InP HEMT with $n^+Al_{0.48}In_{0.52}As/iIn_{0.53}Ga_{0.47}As/iAl_{0.48}In_{0.52}As$ hetero-junction, and Figure 6.14 shows its energy band structure. InPHEMT is composed of a $n^+Al_{0.48}In_{0.52}As/iIn_{0.53}Ga_{0.47}As/iAl_{0.48}In_{0.52}As$ heterojunction semiconductor epitaxial layer formed on a semi-insulating InP substrate with source (S), drain (D), and gate (G) terminals. According to Figure 6.1, the lattice constants of InP, $Al_{0.48}In_{0.52}As$. and $In_{0.53}Ga_{0.47}As$ are equal, and a crystal without lattice defects can be formed. Since semi-insulating InP semiconductor is used as the substrate, it is called InPHEMT. Although InPHEMTs provide high-speed and high-gain characteristics, there are, however, manufacturing and cost issues due to the use of InP semiconductor substrates.

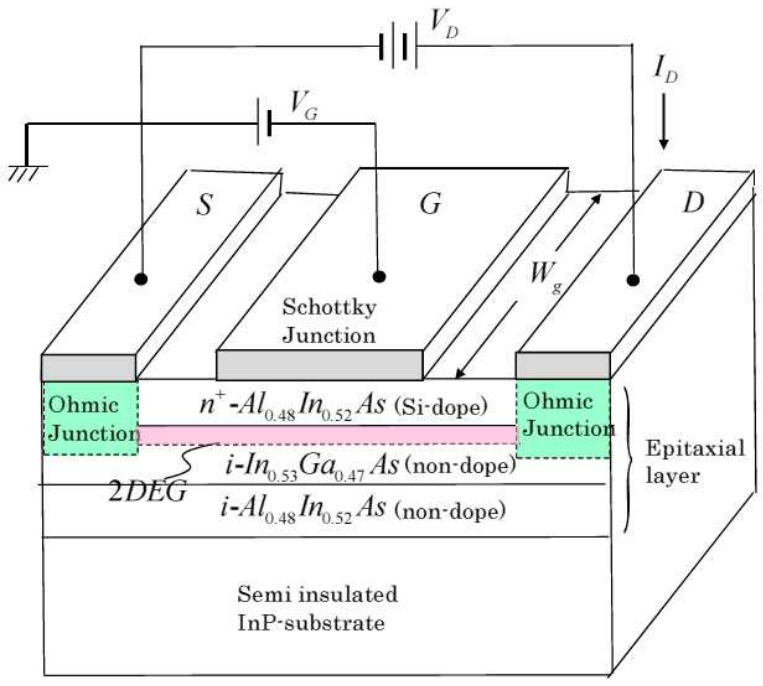

Figure 6.13 Structure model of InPHEMT
($Al_{0.48}In_{0.52}As/In_{0.53}Ga_{0.47}As/Al_{0.48}In_{0.52}As$)

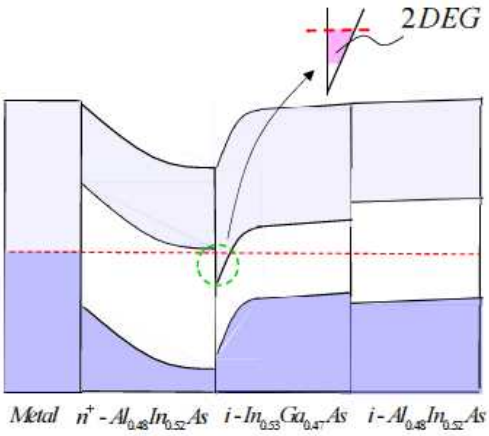

Figure 6.14 Energy band structure of InPHEMT ($Al_{0.48}In_{0.52}As/In_{0.53}Ga_{0.47}As/Al_{0.48}In_{0.52}As$)

6.2.4 Wide Band Gap (WBG) Device

Wide Band Gap (WBG) devices using GaN-based semiconductors have been attracting attention as devices that can provide high power performance in high frequency bands (RF ~ millimeter wave). Table 6.1 shows the physical constants of semiconductors, mainly GaN-based semiconductors. The table also shows data for Si and $GaAs$,

Table 6.1 Physical property constants of semiconductors

	Si	$GaAs$	GaN	AlN	InN	SiC	C Diamond
$E_G(eV)$	1.1	1.4	3.4	6.2	0.7	3.3	5.5
$BV_R(10^8 V/m)$	0.3	0.4	3.3	–	2.0	3.0	4.0
$\theta_\sigma(10^2 W/mK)$	1.5	0.5	2.1	2.9	0.8	4.9	20.9
$\mu_e(m^2/V\cdot s)$	0.15	0.88	0.12	–	0.4	0.1	0.18
$v_e(10^5 m/s)$	1.0	2.0	2.5	2.0	4.2	2.0	2.5

(Data from Ref. [14], p. 24)

From the table, the breakdown voltage BV_R of GaN is more than 8 times higher than that of $GaAs$, and the thermal conductivity θ_σ is more than 4 times higher. On the other hand, the electron mobility μ_e of GaN is smaller

than that of $GaAs$, but the electron saturation velocity v_e is 1.25 times higher, enabling high speed operation at high voltage operation. From the above, it can be said that GaN is a semiconductor material suitable for high-frequency and high-power devices. The band gap energy E_G of GaN is 3.4 V, which is 2.4 times higher than that of $GaAs$ (1.4 V). Therefore, it can be said that GaN is less susceptible to electron-hole pair generation due to thermal excitation, enabling stable device operation up to high temperatures.

Figure 6.15 shows the structure model of a GaN HFET with $Al_xGa_{1-x}N/GaN$ heterojunction as a WBG device. The GaNHFET consists of an epitaxial layer made of $nAl_xGa_{1-x}N/iGaN$ heterojunction semiconductor with source (S), drain (D), and gate (G) terminals. The epitaxial layer is formed on a SiC substrate with excellent thermal conductivity via a buffer layer to absorb distortion caused by differences in lattice constants.

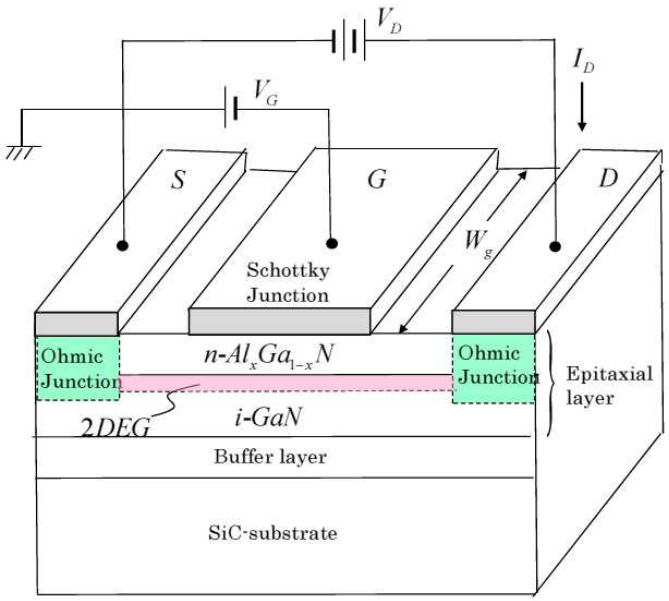

Figure 6.15 Structure model of GaNHFET with $Al_xGa_{1-x}N/GaN$ heterojunction

Figure 6.16 shows its energy band structure. Self-polarization occurs in GaN and $Al_xGa_{1-x}N$ with wurtzite-type crystal structures. Furthermore, when these are heterojunctioned, the difference in lattice constants causes tensile strain, which adds piezoelectric polarization in the $Al_sGa_{1-x}N$. These two

polarization effects generate an electric field at the heterojunction, which changes (curves) the energy band structure as shown in Figure 6.16. As a result, a triangular potential well is formed at the junction, where a channel consisting of 2DEGs is generated. In practice, the $2DEG$ can be considered to be formed by electrons supplied from the S and D terminals during bias wiring. Its behavior when bias is applied can be considered as in the case of HEMT.

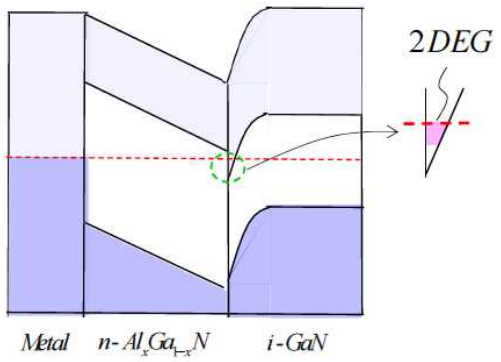

Figure 6.16 Energy band structure of GaNHFET with $Al_xGa_{1-x}N/GaN$ heterojunction

The generation of $2DEG$ is related to the Al composition (x value) of $Al_sGa_{1-x}N$. For example, a high concentration of $2DEG$ can be obtained without adding donors to $Al_xGa_{1-x}N$ (i.e., even as $iAl_xGa_{1-x}N$).

According to Figure 6.2, lattice matching with GaN is possible by using $Al_xIn_{1-x}N$ ($Al_{0.83}In_{0.17}N$) as the barrier layer. Other WBG devices, such as GaNHFETs using $Al_xIn_{1-x}N$, have also been developed.

6.3 Heterojunction Bipolar Transistor (HBT)

HBT (Heterojunction Bipolar Transistor) is a bipolar transistor that uses a heterojunction of different semiconductor materials in the PN junction, and has higher gain and better high frequency performance than the BJT that uses a single Si semiconductor. HBTs include the $GaAsHBT$, which uses a $GaAs$ -based compound semiconductor in the heterojunction, and the $SiGeHBT$, which uses $SiGe$.

Here, we focus on the NPN-type $GaAsHBT$ and describe its structure

and operation. Figure 6.17 shows the structure model of a planar NPN-type $GaAsHBT$. NPN-type $GaAsHBT$ is composed of an $nAl_{0.3}Ga_{0.7}As$ emitter (E) region, a $pGaAs$ base (B) region, and an $nGaAs$ collector (C) region formed on a semi-insulating $GaAs$ substrate. The emitter(E)-base(B) interface is $Al_{0.3}Ga_{0.7}As/GaAs$ heterojunction.

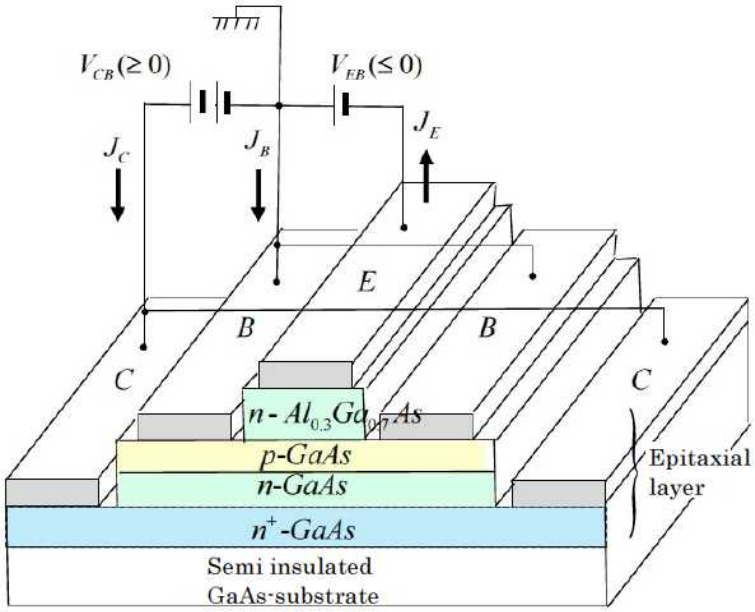

Figure 6.17 Structure model of a planar NPN-type $GaAsHBT$

Figure 6.18 shows the energy band structure of NPN-type $GaAsHBT$. The figure shows the situation when bias is applied.

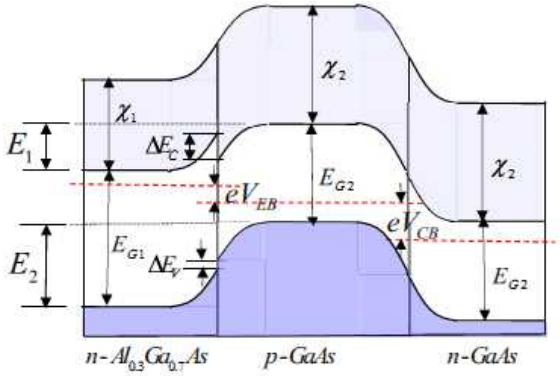

Figure 6.18 Energy band structure of NPN-type $GaAsHBT$ (with bias applied)

Due to the heterojunction between emitter (E) and base (B), the energy difference E_1 at the bottom of the conduction band of E and B is smaller than the energy difference E_2 at the top of the valence band ($E_1 \leq E_2$). Hence, the density of conduction electrons injected from E to B (majority carriers in E and minority carriers in B) is larger than the density of electron holes injected from B to E (majority carriers in B and minority carriers in E).

Figure 6.19 shows the configuration of this HBT and the flow of carriers (conduction electrons and electron holes). Due to the emitter (E)-base (B) heterojunction, the flow of electron holes injected from B to E is smaller than the flow of conduction electrons injected from E to B. This is shown by changing the thickness of the arrows.

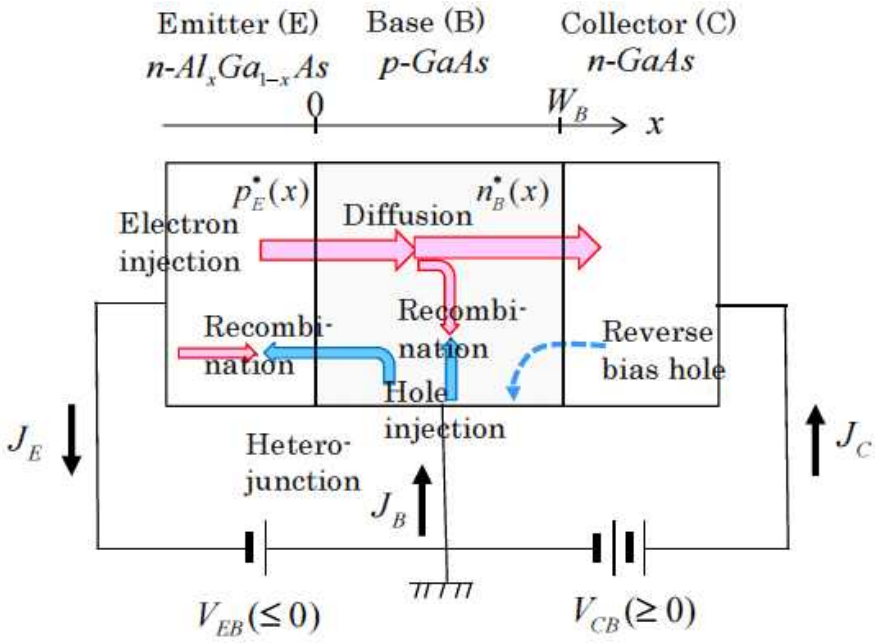

Figure 6.19　HBT configuration and carrier flow

Figure 6.20 shows appearance of current in this HBT. The different carrier (conduction electrons and electron holes) density flows shown in Figure 6.19 result in different magnitudes of current. That is, the emitter current $J_{Eh}(=J_{Bh})$ due to electron holes is smaller than the emitter current J_{Ee} due to conduction electrons. This is also indicated by changing the thickness of the arrow.

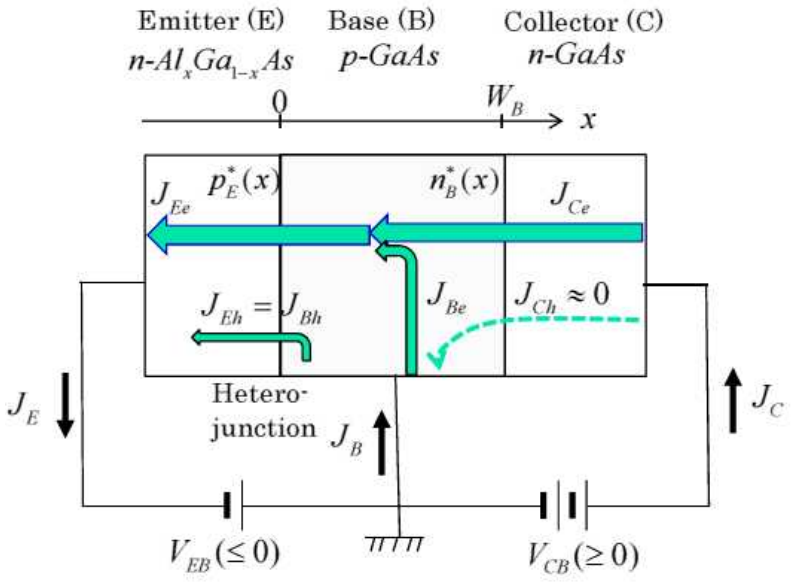

Figure 6.20　Appearance of current in HBT

Here, the common base current gain α and the common emitter current gain β corresponding to equations (3.66) and (3.67) in section 3.4 are given as follows.

$$\alpha = \frac{J_C}{J_E} = \frac{J_{Ce}}{J_{Ee} + J_{Eh}} \tag{6.18}$$

$$\beta = \frac{J_C}{J_B} = \frac{J_{Ce}}{J_{Be} + J_{Bh}} = \frac{J_{Ce}}{J_{Ee} - J_{Ce} + J_{Eh}} \tag{6.19}$$

Where each current symbol is shown in the figure. Due to the heterojunction, the emitter current $J_{Eh}(=J_{Bh})$ by electron holes in the case of HBT is smaller than that of BJT, resulting in larger current gains α and β. This also increases the cutoff frequency f_T.